Experimental Identification of Induction Machine Flux Maps for Traction Applications

Experimental Identification of Induction Machine Flux Maps for Traction Applications

Luisa Tolosano
Dipartimento Energia "G. Ferraris"
Politecnico di Torino
Torino, 10129, Italy
luisa.tolosano@polito.it

Eric Armando
Dipartimento Energia "G. Ferraris"
Politecnico di Torino
Torino, 10129, Italy
eric.armando@polito.it

Sandro Rubino
Dipartimento Energia "G. Ferraris"
Politecnico di Torino
Torino, 10129, Italy
sandro.rubino@polito.it

Fabio Mandrile
Dipartimento Energia "G. Ferraris"
Politecnico di Torino
Torino, 10129, Italy
fabio.mandrile@polito.it

Radu Bojoi
Dipartimento Energia "G. Ferraris"
Politecnico di Torino
Torino, 10129, Italy
radu.bojoi@polito.it

***Abstract*—Nowadays the permanent magnet machines are a widespread solution in the automotive field. However, the induction machine (IM) represents a valid solution as it is rare-earth free and does not have induced stator back-emf in case of inverter turn-off. Regardless of the machine type, identification procedures are needed for torque control calibration and for optimal machine utilization in terms of efficiency and maximum torque production under inverter current and voltage constraints. For synchronous machines, a common and consolidated practice is to obtain the machine flux maps (current-to-flux relationship) in the rotor (*d,q*) frame using calibrated Finite Element Analysis (FEA) or experimental procedures. However, to the best of the authors' knowledge, the literature does not report an experimental approach able to obtain the flux maps for IMs. Therefore, this paper proposes an experimental procedure to obtain the IM flux maps in (*d,q*) rotor flux frame for inverter supply and real operating conditions. In addition, the proposed procedure is able to obtain the parameters of the IM equivalent circuit with no need of additional tests. Experimental validation is provided for a 4-poles IM rated 10 kW, 200 Hz.**

Keywords*—induction motor, steady-state (d,q) flux maps, electric parameters identification

I. Introduction

In the last years, the attention of the traction application field has been focused on the permanent magnet synchronous machines (PMSM) thanks to their high torque density and high efficiency. Recently, the perspective has changed because of the magnets cost increase and possible shortages, making the PMSM less attractive. In this scenario, the induction machine (IM) can still play a primary role [1] as it is magnet-free and does not induce any voltage at high speed in case of sudden inverter turn-off. The knowledge of the steady-state flux maps together with the equivalent circuit parameters in real operating conditions (in terms of temperature, frequency, and saturation) is essential to achieve optimal torque control up to the maximum speed [2]–[5]. Indeed, an error in the estimation of the parameters can lead to the derating of the control performance, with a significant decrease in the torque capability of the machine. The experimental identification of the IM steady-state flux maps $\lambda_d(i_d, i_q)$, $\lambda_q(i_d, i_q)$ defined in the rotor flux (*d,q*) frame is not trivial as the rotor flux linkage position cannot be measured. Therefore, the experimental procedures proposed in the literature for synchronous machines [6] cannot be used.

Concerning the knowledge of the IM equivalent circuit electric parameters (stator and rotor resistances, stator and rotor leakage inductances, magnetizing inductance), the literature reports various techniques to obtain them from numerical analysis and experimental procedures. The ones based on FEA and numerical analysis [7]–[9] are feasible only if the geometry and the materials are known. The motor's final user can identify the machine parameters only by means of experimental procedures. The IEEE 112 standard outlines the procedure to obtain the main IM parameters through the well-known no-load and locked-rotor tests [10]. Other options to obtain the equivalent circuit parameters leverage the features provided by the digital control. These procedures are implemented directly by the drive digital controller and they can be classified as online or offline. The online solutions are implemented during the drive operation, allowing real-time adjustment of machine parameters. The off-line solutions are implemented before the drive operation. This paper focuses on off-line procedures.

State-of-the-art methods include self-commissioning (SC) procedures [11], and they have quite stringent requirements. In SC procedures, the parameters are evaluated automatically by the motor controller in order to perform the machine torque control. Both ac or dc excitations can be applied through the inverter and the parameters identification is based on a sequence of tests. When the machine is allowed to rotate, the identification of the machine's parameters is simplified [12]. The measurements with the machine running at no-load are performed at low speed to minimize the impact of iron and

mechanical losses. The major problem that arises with these off-line procedures is the impact of the inverter nonlinearities that make inaccurate the parameters identification based on the reconstructed inverter voltages. Indeed, the impact of the inverter voltage drops and dead-time effects is significant, especially at low speed. Moreover, the available procedures are not performed within the supply and operating conditions that correspond to the real machine operation. As a result, none of them can map the behavior of the parameters in the operative frequency range. Indeed, to identify exhaustively the induction machine's parameters, both the current- and the slip frequency- ranges must be explored. The full current range is needed to explore properly the machine saturation, while the full slip frequency range is mandatory for the proper characterization of the frequency-dependent parameters, such as the rotor resistance and magnetizing inductance. A current - slip frequency-based parameter identification procedure was proposed in [13]. This solution is based on fitting steady-state current measurements to the stator current locus for various slip frequencies in the stator flux linkage reference frame. The magnetic parameters can be identified if the stator flux linkage amplitude is kept constant by a regulator during the data collection. However, this method intrinsically requires a flux regulator and flux linkage estimator that is sensitive to the inverter dead-time effects.

Therefore, this paper proposes an experimental identification procedure that is able to accurately obtain the induction machine steady-state flux maps and map the IM electric parameters in the real machine operating conditions. Compared to the state-of-the-art procedures, the proposed one has the following advantages:

- a single test is performed using the target inverter of the motor application;
- the proposed procedure identifies the IM flux-maps in the rotor flux (d,q) frame without the need of a rotor flux observer, differently from previous solutions [13], [14];
- the procedure allows the identification of all the IM parameters in actual machine operating conditions in terms of slip and current.

The paper is organized as follows. Section II reports the IM model on which the identification procedure is based. The experimental identification procedure is presented in Section III, while the required post-processing elaboration with the main results are reported in Section IV. Finally, Section V provides the conclusions.

II. IM Electromagnetic Model

To better understand the theoretical background on which the identification procedure relies, the electromagnetic model of a generic three-phase IM with an arbitrary number of pole pairs p is reported. Moreover, a sinusoidal distribution of the stator windings is assumed, i.e., they interact with each other and the squirrel-cage rotor only through the spatial-fundamental component of the airgap field, thus neglecting the effects of the high order spatial harmonics. For simplicity, the iron losses are neglected. In the following, the IM electromagnetic model is reported using two different system coordinates represented in Fig. 1 : *i)* a generic (x,y) rotating frame and *ii)* a stator current (d_i, q_i) frame, i.e., the d_i-axis is defined by the stator current vector. The choice of this orientation will simplify the elaboration on which the identification method is based on.

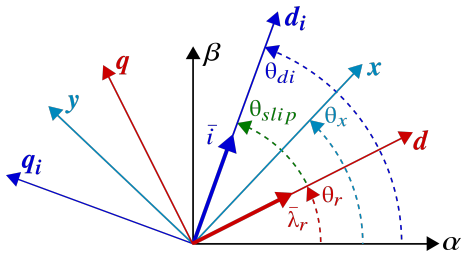

Fig. 1. Definition of rotor flux (d,q) frame, generic frame (x,y) and stator current (d_i, q_i) frame.

A. Electromagnetic model in generic rotating coordinates

According to the literature [15], the IM electric model in generic rotating coordinates (x,y) is computed as:

$$\bar{v}_{xy} = R_s \cdot \bar{i}_{xy} + j \cdot \omega_{xy} \cdot \bar{\lambda}_{xy} + \frac{d}{dt}\bar{\lambda}_{xy} \tag{1}$$

$$\bar{v}_{r,xy} = R_r \cdot \bar{i}_{r,xy} + j \cdot (\omega_{xy} - \omega_r) \cdot \bar{\lambda}_{r,xy} + \frac{d}{dt}\bar{\lambda}_{r,xy} \tag{2}$$

where:

- v, i and λ are the stator voltage, current and flux linkage vectors. The subscript *"r"* is used for rotor quantities;
- R_s and R_r are stator and rotor phase resistances;
- ω_{xy} is the x-axis rotational speed, ω_r is the rotor electrical speed evaluated as $\omega_r = p \cdot \omega_m$ (ω_m is the rotor mechanical speed, p the number of pole pairs).

The rotor and stator magnetic (x,y) models of the machine (current-to-flux relationships), are difficult to express analytically due to magnetic saturation. However, if assuming the machine magnetizing inductance depends on the (x,y) currents, the magnetic (x,y) model can be expressed as:

$$\bar{\lambda}_{xy} = L_{ls} \cdot \bar{i}_{xy} + L_m(i_{mx}, i_{my}) \cdot \bar{i}_{m,xy} \tag{3}$$

$$\bar{\lambda}_{r,xy} = L_{lr} \cdot \bar{i}_{r,xy} + L_m(i_{mx}, i_{my}) \cdot \bar{i}_{m,xy} \tag{4}$$

where L_m is the magnetizing inductance and L_{ls} and L_{lr} are the stator and the rotor leakage inductances, respectively, and $\bar{i}_{m,xy} = \bar{i}_{xy} + \bar{i}_{r,xy}$ is the magnetizing current.

The electromagnetic torque defined in the generic (x,y) rotating frame is expressed as:

$$T_e = 3/2 \cdot p \cdot (\lambda_x \cdot i_y - \lambda_y \cdot i_x) = 3/2 \cdot p \cdot (\bar{\lambda}_{xy} \times \bar{i}_{xy}) \tag{5}$$

It is noted how the machine torque is proportional to the outer product between the stator flux linkage vector and stator current vector. The measured torque will be adopted in the

identification procedure as a benchmark value to demonstrate the effectiveness of the proposed method.

The elaboration needed to obtain the useful flux-to-current relationships involving also the slip speed ω_{slip} (computed as $\omega_{slip} = 2 \cdot \pi \cdot f_{slip}$) is not trivial. The flux-to-current equations are evaluated combining together the steady-state stator and rotor electric and magnetic equations. The final equations are reported in the following:

$$\begin{cases} \lambda_x = k_1 \cdot I_x + k_2 \cdot I_y \cdot \omega_{slip} \\ \lambda_y = k_1 \cdot I_y - k_2 \cdot I_x \cdot \omega_{slip} \end{cases} \tag{6}$$

where $k_1 = [(R_r^2 \cdot L_m \cdot K_r)/(R_r^2 + (\omega_{slip} \cdot L_r)^2) + \sigma \cdot L_s]$ and $k_2 = (R_r \cdot L_m^2)/(R_r^2 + (\omega_{slip} \cdot L_r)^2)$ are the two coefficients obtained in the elaboration.

B. Electromagnetic model in stator current vector coordinates

In the (d_i, q_i) reference frame aligned with the stator current vector, the IM equations are the same as in (1)–(5), with the subscript "dq_i" instead of the generic "xy". The adoption of the (d_i, q_i) reference frame, i.e., $\bar{i}_s = I_s + j0$, enables the simplification of the steady-state flux-to-current relationship (6) as follows:

$$\begin{cases} \lambda_{di} = k_1 \cdot I \\ \lambda_{qi} = -k_2 \cdot I \cdot \omega_{slip} \end{cases} \tag{7}$$

Adopting (7) in the steady-state form of stator voltage equations (1) leads to the following expressions:

$$\begin{cases} v_{di} = R_s \cdot I - \omega_{dqi} \cdot \lambda_{qi} \\ \quad\; = R_s \cdot I + (\omega_r + \omega_{slip}) \cdot (k_2 \cdot I \cdot \omega_{slip}) \\ v_{qi} = \omega_{dqi} \cdot \lambda_{di} \\ \quad\; = (\omega_r + \omega_{slip}) \cdot (k_1 \cdot I) \end{cases} \tag{8}$$

where the stator synchronous speed ω_{dqi} is expressed as $\omega_{dqi} = (\omega_r + \omega_{slip})$. Equation (8) for motor and generator operation can be expressed as:

$$\begin{cases} v_{di,M} = R_s \cdot I - (\omega_r + |\omega_{slip}|)\lambda_{qi,M} \\ v_{qi,M} = (\omega_r + |\omega_{slip}|) \cdot \lambda_{di,M} \end{cases} \tag{9}$$

$$\begin{cases} v_{di,G} = R_s \cdot I + (\omega_r - |\omega_{slip}|)\lambda_{qi,M} \\ v_{qi,G} = (\omega_r - |\omega_{slip}|) \cdot \lambda_{di,M} \end{cases} \tag{10}$$

It must be noticed that, leveraging the motor-generator q_i-axis symmetry, the stator flux components in generator mode $\lambda_{dqi,G} = \lambda_{di,G} + j \cdot \lambda_{qi,G}$ have been properly replaced with the motor ones $\lambda_{dqi,G} = \lambda_{di,M} - j \cdot \lambda_{qi,M}$. In this way, the variables adopted in the generator mode equation are consistent with the ones in the motor mode. In order to retrieve the (d_i, q_i) flux components, the motor and generator voltage equations are combined together. The final flux-to-voltage relationship becomes:

$$\begin{cases} \lambda_{di,M} = \dfrac{v_{qi,M} + v_{qi,G}}{2 \cdot \omega_r} \\ \lambda_{qi,M} = \dfrac{v_{di,G} - v_{di,M}}{2 \cdot \omega_r} \end{cases} \tag{11}$$

Leveraging both motor and generator modes allows the elimination of the effects of voltage drops on stator resistance in the voltage measurements [6]. Moreover, by calculating (5) in (d_i, q_i) reference frame, the torque expression becomes:

$$T_e = -\frac{3}{2} \cdot p \cdot \lambda_{qi} \cdot i = \frac{3}{4 \cdot \omega_r} \cdot p \cdot (v_{di,M} - v_{di,G}) \cdot I \tag{12}$$

It must be highlighted that the (d_i, q_i) flux components in (11) and the torque in (12) can be directly obtained from the voltage and speed measurement via the straightforward procedure explained in the following section.

III. Experimental Identification Procedure

The proposed procedure can identify not only the torque and steady-state equivalent (*d,q*) flux maps of the IM, but also the electric parameters, namely the stator and rotor resistances (R_s, R_r), leakage inductances (L_{ls}, L_{lr}) and the magnetizing inductance (L_m). Unfortunately, the position of the rotor *d*-axis can be provided only by a flux observer that requires the knowledge of the machine parameters to be identified. Therefore, the solution adopted to overcome this issue is to define a reference frame (d_i, q_i) where the stator current vector defines the d_i-axis, rotating at the synchronous speed ω_{dqi} previously defined.

For the exhaustive mapping of the machine and the identification of the electric parameters, a complete exploration of both the current and slip frequency ranges must be performed. In order to characterize the IM, the test points are chosen according to a predefined current- and slip frequency- meshgrid taking into account the limits of current amplitude and slip frequency. The two limits are related to the machine under test since the stator current amplitude is defined following the machine overload capability, while the slip frequency should not overcome a maximum reasonable value. The final settings adopted to generate the maps for the motor under test are the following: the current amplitude varies between 2 A and 28 A, with a step of 2 A, the slip frequency varies between 0 Hz and 15 Hz, with a step of 0.5 Hz. This leads to a mesh of 465 testing points. The maximum current amplitude corresponds to an overload of 200 %, since the rated current is 14 A peak.

The proposed procedure requires the test rig in Fig. 2, where the three-phase power converter feeding the IM under test is supplied by a bidirectional dc source. The flowchart of

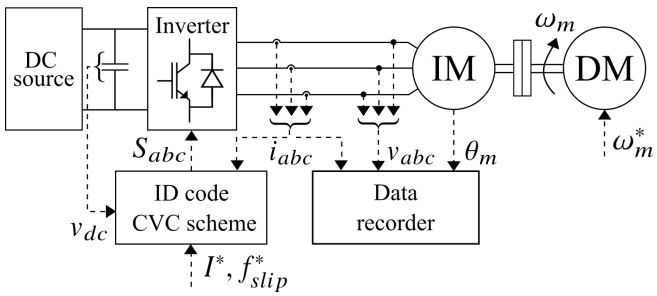

Fig. 2. Scheme of the test rig.

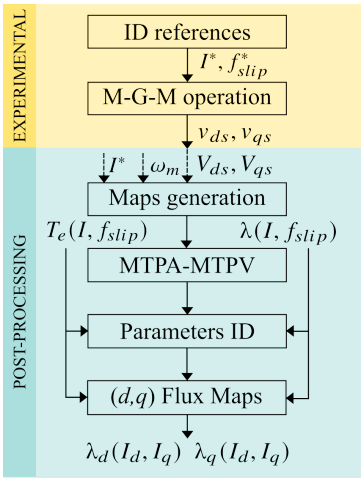

Fig. 3. Flow diagram of the proposed procedure.

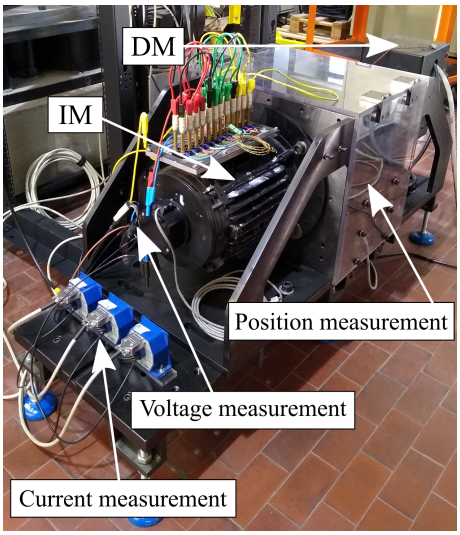

Fig. 4. View of the experimental test rig.

the proposed procedure is shown in Fig. 3. The experimental validation has been performed on 4-poles IM rated 10 kW, 200 Hz, adopting the switching and sampling frequencies equal to 8 kHz. A view of the experimental test rig is shown in Fig. 4.

The measurements of phase currents, line-to-line voltages, rotor position and torque, have been collected by the data recorder HBM Gen4tB. The digital controller is the fast-prototyping board dSPACE MicroLabBox, while the control algorithm has been fully implemented in C-code. It is highlighted that the digital controller does not require specific features: any used for three-phase electric drives can be adopted.

Using a driving machine (DM), the speed of the IM under test is set at a reference value of 1000 r/min (below 25% of rated speed) that allows sensing the machine voltages properly, and at the same time, makes the iron losses negligible. Since the speed adopted to perform the test is relatively low, in theory a proper evaluation of the inverter nonlinearities effects, especially the dead-time one, must be performed. This care is of primary importance if a direct voltage measurement on the stator windings is not possible and therefore the voltage components needed by the flux and torque computations must be reconstructed from the measured dc link voltage and inverter duty-cycles. In this case, the voltage error due to the inverter dead time effects may become important [16].

Once a constant rotational speed has been reached, the current-slip test point $(I(k)^*, f^*_{slip}(w))$ is imposed. The identification procedure requires both motor (M)-($f^*_{slip} > 0$) and generator (G)-($f^*_{slip} < 0$) operation to exploit the compensation of stator resistance voltage drops as in [6]. At steady-state operating conditions (in each mode), the instantaneous line-to-line voltages are measured using a data recorder, thus avoiding the error on the reconstructed voltages. The voltage components, (v_{di-kw}, v_{qi-kw}) in stator current reference frame are evaluated in real-time and their values are averaged on a mechanical revolution to get the average values (V_{di-kw}, V_{qi-kw}). As described in [6], a break time interval between two consecutive test points is needed to avoid excessive heating.

The (V_{di-kw}, V_{qi-kw}), together with the measured mechanical speed ω_m and the reference current amplitude I^*, are used to generate the torque and flux components amplitude, i.e., $T_e(I, f_{slip})$, $\lambda_{di}(I, f_{slip})$, and $\lambda_{qi}(I, f_{slip})$, adopting (11) and (12). The experimental flux amplitude $\lambda(I, f_{slip})$ and torque maps for the motor under test are shown in Fig. 5 and in Fig. 6. As expected, the larger flux amplitude corresponds to the high current - low slip frequency range, where the phase-shift between the rotor flux vector and the stator current vector is low. As the slip increases, this phase-shift increases as well leading to a reduction of the total flux amplitude. The typical torque production of the IM for different current amplitudes is depicted in Fig. 6. The highest torques are delivered from the machine with a slip frequency in the range (1÷3.5) Hz. To get confirmation of the torque map results, the torque transducer HBK T40B has been mounted along the mechanical coupling between IM under test and DM. The absolute deviation between the measured torque value and the one from (12) is shown in Fig. 7. The absolute torque error is negligible, also considering that the contribution of mechanical torque losses have not been taken into account.

IV. Post-Processing Elaboration

The post-processing procedure required to retrieve the steady-state equivalent (*d,q*) flux maps and the equivalent circuit parameters is based on the torque and flux maps, i.e., $T_e(I, f_{slip})$, $\lambda_{di}(I, f_{slip})$, and $\lambda_{qi}(I, f_{slip})$. Since the perfect orientation of the current vector in the (d_i, q_i) reference frame is quite challenging, a re-alignment procedure with a rotation transformation may be needed on the raw data, using post-processing functions of the data recorder. Once the data have been refined, i.e., $I_{qi} = 0$, they can be further manipulated. The first task is the identification of the machine control loci, i.e.,

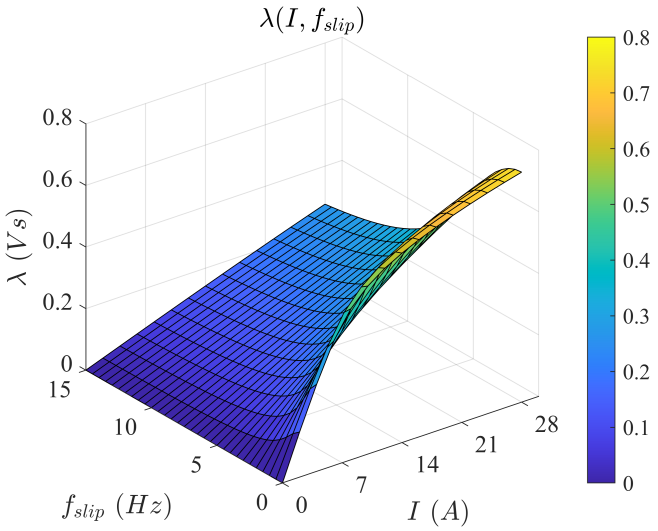

Fig. 5. IM flux map $\lambda(I, f_{slip})$.

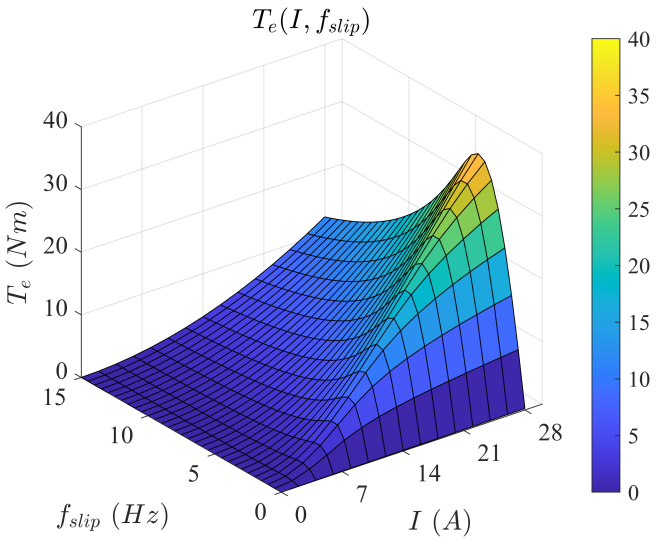

Fig. 6. IM torque map $T_e(I, f_{slip})$.

the maximum torque per ampere (MTPA), and the maximum torque per volt (MTPV). Both these evaluations are quite straightforward since the two fundamental variables on which the identification of MTPA and MTPV are respectively based (current and flux amplitudes), are directly accessible. For each investigated torque level, all the combinations of current amplitude and slip frequency are extracted from $T_e(I, f_{slip})$. The MTPA locus is defined by finding the minimum current amplitude for every torque level. The MTPV locus can be obtained from the recognition on $\lambda_s(I, f_{slip})$ of the minimum flux amplitude for every torque level. In this preliminary phase, it must be noticed that the control loci are known only in terms of the slip frequency f_{slip}, stator flux λ and current I amplitudes. The knowledge of the MTPA locus is useful when dealing with high-efficient machine control strategies, while the MTPV locus will be exploited for the identification of the

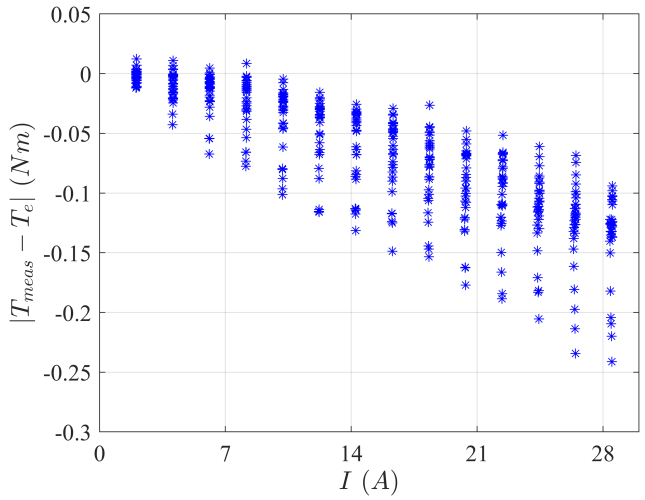

Fig. 7. IM torque error map.

equivalent circuit parameters. The steps required to identify the parameters exploits the machine equations in the stator (d_s, q_s) frame, i.e., the magnetic d_s-axis is assumed coincident with that of the stator flux linkage vector λ [17], and they can be organized as follows.

- The stator quadrature current can be derived inverting the torque equation. The direct current is then obtained using the i_{MTPV} as follows:

$$i_{qs,MTPV} = \frac{T_e}{3/2 \cdot p \cdot \lambda_{MTPV}} \tag{13}$$

$$i_{ds,MTPV} = \sqrt{i^2_{MTPV} - i^2_{qs,MTPV}} \tag{14}$$

- The first coefficient that can be directly derived is σL_s that is used to weight the effect of the stator current on the stator flux production, as described in (15) that is valid for any reference frame:

$$\bar{\lambda} = k_r \cdot \bar{\lambda}_r + \sigma L_s \cdot \bar{i} \tag{15}$$

The (d_s, q_s) current components from (15) are the following:

$$\begin{cases} i_{ds} = \dfrac{\lambda - k_r \cdot \lambda_r \cdot \cos(\delta)}{\sigma L_s} \\ i_{qs} = \dfrac{k_r \cdot \lambda_r \cdot \sin(\delta)}{\sigma L_s} \end{cases} \tag{16}$$

The ratio between the direct and the quadrature current components becomes as:

$$\frac{i_{ds}}{i_{qs}} = \frac{\lambda}{k_r \cdot \lambda_r \cdot \sin(\delta)} - \frac{1}{\tan(\delta)} \tag{17}$$

In (17) k_r, λ_r, δ are unknown quantities that can not be obtained from the raw data, but from the torque equation obtained adopting (15) in (5), as follows:

$$T_e = 3/2 \cdot p \cdot \frac{k_r}{\sigma L_s} \cdot \lambda_r \cdot \lambda \cdot \sin(\delta) \tag{18}$$

where the σL_s coefficient is employed. Reversing (18) to obtain $k_r \cdot \lambda_r \cdot \sin(\delta)$ and substituting its expression in (17) leads to:

$$\frac{i_{ds}}{i_{qs}} = \frac{3}{2} \cdot p \cdot \frac{\lambda^2}{T_e \cdot \sigma \cdot L_s} - \frac{1}{\tan(\delta)} \tag{19}$$

Finally, exploiting the fact that the machine load angle of the IM in MTPV is always known and equal to 45°, i.e., $\tan(\delta) = 1$, and, since all the quantities in (19) are known in MTPV, the $(\sigma L_s)_{MTPV}$ can be derived as follows:

$$(\sigma L_s)_{MTPV} = \frac{3}{2} \cdot p \cdot \frac{\lambda^2}{T_e \cdot [(i_{ds}/i_{qs}) + 1]} \tag{20}$$

where $T_e, \lambda, i_{ds}, i_{qs}$ are the value at MTPV operation.

- The stator inductance curve at no-load conditions L_{s0}, i.e., at zero slip frequency (zero torque), can be directly computed from the experimental maps using:

$$L_{s0} = \frac{|\lambda(f_{slip} = 0)|}{|I(f_{slip} = 0)|} \tag{21}$$

- The saturated profile of the stator inductance in MTPV $L_{sMTPV}(i_{d,MTPV})$ function of the magnetizing current in (d,q) frame, can be obtained with an interpolation on the no-load profile $L_{s0}(I(f_{slip} = 0))$.
- The overall leakage factor σ_{MTPV} can be finally obtained from the following ratio:

$$\sigma_{MTPV} = \frac{(\sigma L_s)_{MTPV}}{L_{sMTPV}} \tag{22}$$

- The rotor-to-stator coupling factors k_r and k_s are obtained with the same procedure. The usual hypothesis of dividing equally between stator and rotor the short-circuit inductance L_{cc} to obtain $L_{ls} = L_{lr} = L_{lx} = L_{cc}/2$ has been adopted. In this way the coupling factors can be generally indicated with k_x, as they are equal, and evaluated as follows:

$$k_{x,MTPV} = \sqrt{1 - \sigma_{MTPV}} \tag{23}$$

- The value of the leakage inductance L_{lx} is finally evaluated as:

$$L_{lx} = \frac{(\sigma L_s)_{MTPV}}{1 + k_x} \tag{24}$$

- The magnetizing inductance profile at no-load L_{m0} can be directly obtained given (21) and (24) as:

$$L_{m0} = L_{s0} - L_{lx} \tag{25}$$

All the quantities listed can be considered accurate only in the MTPV locus where their values have been obtained. Nevertheless, since some of these variables can not be derived from any other information available in this stage of the identification procedure, they will anyway adopted in the following procedure. To map the behavior of the IM in the (d,q) reference frame further data manipulation is required, and it is reported in the following.

- The load angle map δ_{map} can be obtained reverting (19) as:

$$\delta_{map} = \arctan\left[\left(\frac{3}{2} \cdot p \cdot \frac{\lambda^2}{T_e \cdot (\sigma L_s)_{MTPV}} - \frac{i_{ds}}{i_{qs}}\right)^{-1}\right] \tag{26}$$

where T_e and λ are the torque and flux amplitude maps obtained from the experimental procedure.

- The procedure to obtain $L_{m,map}$ is the same adopted previously for the saturated behavior. Here the magnetizing inductance function of the d-axis current map $L_{m,map}(i_{d,map})$ can be obtained with an interpolation on the no-load profile $L_{s0}(I(f_{slip} = 0))$.
- The rotor-to-stator coupling factor map $k_{x,map}$ is obtained with its conventional formula using the value of the leakage inductance previously evaluated, with the hypothesis that the latter parameter does not go under saturation phenomena:

$$k_{x,map} = \frac{L_{m,map}}{L_{m,map} + L_{lx}} \tag{27}$$

- The (d,q)-axes inductance maps are evaluated as follows:

$$\begin{cases} L_{d,map} = L_{m,map} + L_{lx} \\ L_{q,map} = L_{lx} \cdot (1 + k_{x,map}) \end{cases} \tag{28}$$

where the contribution of magnetizing inductance is present only in the direct axis, while in the quadrature one only the leakage inductance is practically present.

- The steady-state equivalent (d,q) flux maps in Fig. 8a and Fig. 8b can be obtained exploiting the inductance maps just evaluated:

$$\begin{cases} \lambda_{d,map} = L_{d,map} \cdot i_{d,map} \\ \lambda_{q,map} = L_{q,map} \cdot i_{q,map} \end{cases} \tag{29}$$

It is highlighted that the test points have been generated following a polar definition based on current amplitude and slip frequency, i.e., angle, resulting in polar maps. In Fig. 8c, the saturated behavior of the magnetizing inductance can be appreciated in the d-axis flux profile, while, the linear behavior in the q-axis is guaranteed by its dependence on the leakage inductance only. The knowledge of the steady-state equivalent (d,q) flux maps together with the (d,q) current components enables the evaluation of the electromagnetic torque map shown in Fig. 8d.

- The rotor flux map $\lambda_{r,map}$ is evaluated as the product between the magnetizing inductance L_{m0} at no-load and the d-axis current map as follows:

$$\lambda_{r,map} = L_{m0} \cdot i_{d,map} \tag{30}$$

- The rotor time constant $\tau_{r,map}$ can be evaluated exploiting the following expression:

$$\tau_{r,map} = \frac{1}{\omega_{slip,map}} \cdot \frac{i_{q,map}}{i_{d,map}} \tag{31}$$

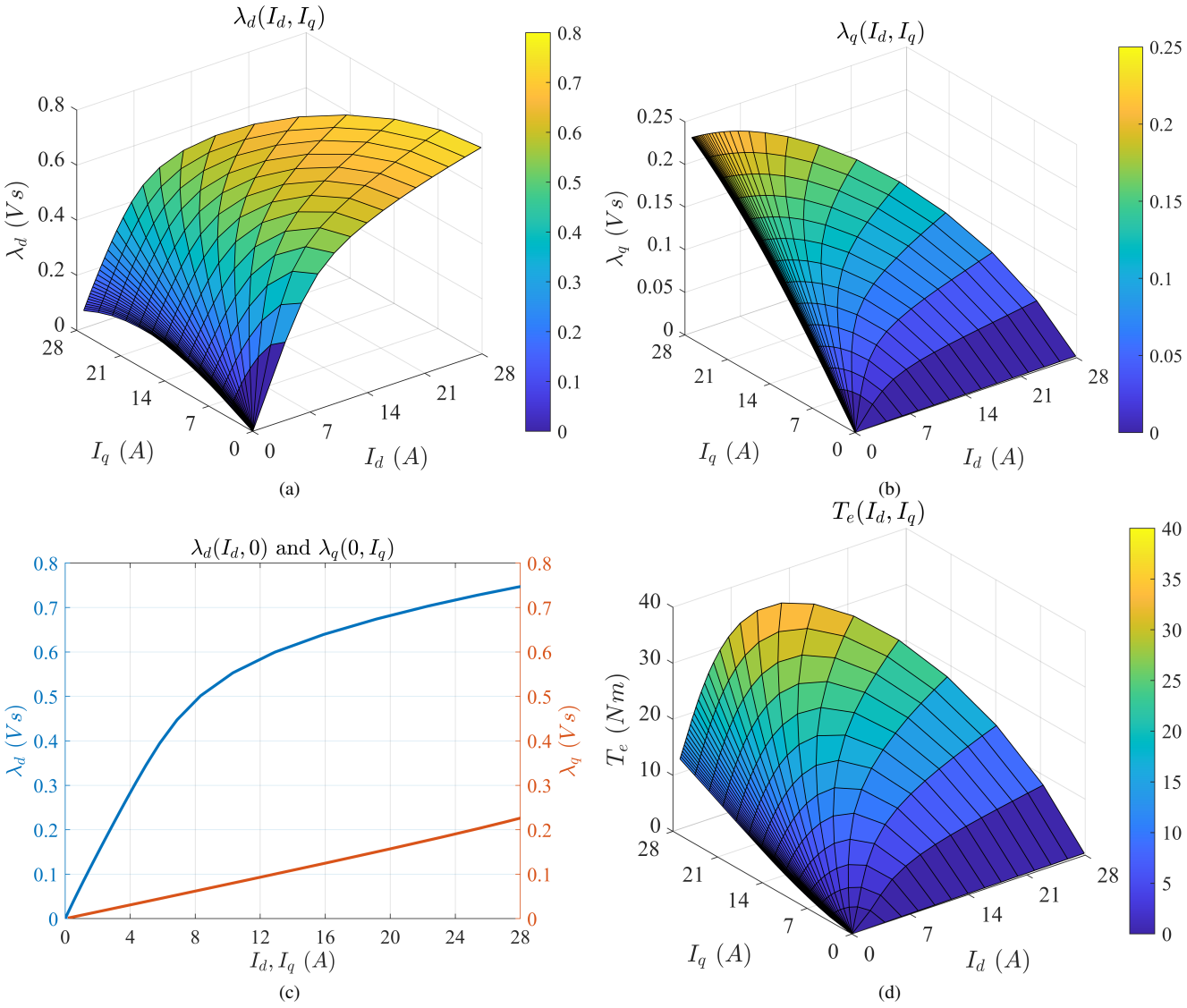

Fig. 8. IM maps: a) $\lambda_d(i_d, i_q)$, b) $\lambda_q(i_d, i_q)$, c) $\lambda_d(I_d, 0)$ and $\lambda_q(0, I_q)$, d) IM torque map.

- The rotor resistance R_r can be evaluated exploiting the rotor time constant and the rotor inductance previously evaluated as in following expression:

$$R_{r,map} = \frac{L_{m0} + L_{lx}}{\tau_{r,map}} \tag{32}$$

- The behavior of the rotor current $i_{r,map}$ in the explored current-slip frequency ranges can be obtained exploiting the machine equation. In (d,q) frame the rotor current can be evaluated as in the following:

$$i_{r,map} = k_{x,map} \cdot i_{q,map} \tag{33}$$

- The overall leakage factor map σ_{map} can be obtained from its usual expression:

$$\sigma_{map} = 1 - k^2_{x,map} \tag{34}$$

- Finally, the stator resistance R_s can be evaluated directly exploiting the machine voltage equations (9) and (10) as:

$$R_s = \frac{v_{di,M} + v_{di,G} + 2 \cdot |\omega_{slip}| \cdot \lambda_{qi}}{2 \cdot I} \tag{35}$$

  It is highlighted that a reasonable value of the stator resistance is obtained only for the high current amplitude measurement where the resistive voltage drop is significant.

A comparison between the equivalent circuit parameters obtained with the IEEE 112 Std and the proposed procedure is reported in Table 1. The parameters have been obtained for machine rated conditions corresponding to a stator current of 14 A peak.

The consistency between the results obtained with the two methods can be appreciated for stator resistance and magnetizing inductance. In contrast, the deviation between the

TABLE I
EQUIVALENT CIRCUIT PARAMETERS COMPARISON

		IEEE 112 Std	Proposed procedure
R_s	Ω	0.598	0.619
R_r	Ω	0.396	0.336
L_{lx}	mH	3.82	4.21
L_m	mH	56.2	55.9
$L_{m,unsat}$	mH	68.4	69.1

values of leakage inductance and rotor resistance is explained by the exploration of the low current-slip frequency ranges. In fact, the value of the leakage inductance defined with the IEEE procedure is affected by saturation: the assumption that this parameter does not go under saturation is therefore not valid. The lower value of rotor resistance is due to its evaluation in the low-frequency range where the skin effect does not affect the resistance value.

The main contribution of the proposed procedure, beyond the definition of the steady-state equivalent (d,q) flux maps, is the investigation of the behavior of the rotor resistance and time constant, i.e., $R_{r,map}$ and $\tau_{r,map}$, in the operative frequency range. The obtained results is of particular interest for these variable because, to the best of the author's knowledge, the proposed procedure is the only one present in the literature able to perform this kind of evaluation.

V. CONCLUSION

This paper proposes an innovative procedure for the magnetic identification of the IM, allowing also the computation of the equivalent circuit parameters through post-processing elaboration. With respect to existing testing procedures, the values of the equivalent circuit parameters are obtained in realistic machine operating conditions, making them useful for the calibration of the torque control in the entire speed range. The proposed solution is applicable to any IM and it requires an experimental setup with accurate speed, current and voltage measurements, to completely identify the parameters in the operative frequency range. The machine under test is supplied by its target inverter and the machine control does not need a flux observer as the adopted synchronous reference frame is defined by the stator current vector.

Different rotational frame with unique properties have been exploited to carry out this procedure. The (d_i, q_i) frame has been used to perform the experimental identification in order to control both the current amplitude and the slip frequency. The (d_s, q_s) frame has been adopted to exploit its peculiarity in the MTPV locus to identify some basic parameter. In the end the target (d, q) frame is the one in which the main quantities have been described.

The adoption of the proposed procedure to identify the machine parameters can be useful in several application, such as preliminary machine characterization in FEA environment and the development of IM high-performance torque control solutions.

ACKNOWLEDGMENT

The authors would like to acknowledge the financial support from the Power Electronics Innovation Center (PEIC) of Politecnico di Torino (www.peic.polito.it).

REFERENCES

[1] R. Thomas, H. Husson, L. Garbuio, and L. Gerbaud, "Comparative study of the Tesla Model S and Audi e-Tron Induction Motors", 17th Conference on Electrical Machines, Drives and Power Systems, pp. 1–6, July 2021.

[2] Kim, Sang-Hoon and Sul, Seung-Ki, "Maximum torque control of an induction machine in the field weakening region", IEEE Transactions on Industry Applications, vol. 31, pp. 787–794, July 1995.

[3] M. Mengoni, L. Zarri, A. Tani, G. Serra, and D. Casadei. "A Comparison of Four Robust Control Schemes for Field-Weakening Operation of Induction Motors", IEEE Transactions on Power Electronics, vol. 27, pp. 307–320, Jan. 2012.

[4] A. Amerise, M. Mengoni, L. Zarri, A. Tani, S. Rubino and R. Bojoi, "Open-ended induction motor drive with a floating capacitor bridge at variable DC link voltage," 2017 IEEE Energy Conversion Congress and Exposition (ECCE), 2017, pp. 3591–3597.

[5] S. Rubino, R. Bojoi, F. Mandrile and E. Armando, "Modular Stator Flux and Torque Control of Multiphase Induction Motor Drives" 2019 IEEE International Electric Machines & Drives Conference (IEMDC), 2019, pp. 531–538.

[6] E. Armando, R. Bojoi, P. Guglielmi, G. Pellegrino, and M. Pastorelli, "Experimental Identification of the Magnetic Model of Synchronous Machines", IEEE Transactions on Industry Applications, vol. 49, pp. 2116–2125, Sept. 2013.

[7] A. Boglietti, A. Cavagnino, and M. Lazzari, "Computational Algorithms for Induction-Motor Equivalent Circuit Parameter Determination—Part I: Resistances and Leakage Reactances", IEEE Transactions on Industrial Electronics, vol. 58, pp. 3723–3733, Sept. 2011.

[8] A. Boglietti, A. Cavagnino, and M. Lazzari, "Computational Algorithms for Induction Motor Equivalent Circuit Parameter Determination—Part II: Skin Effect and Magnetizing Characteristics", IEEE Transactions on Industrial Electronics, vol. 58, pp. 3734–3740, Sept. 2011.

[9] M.H. Haque, "Determination of NEMA Design Induction Motor Parameters From Manufacturer Data", IEEE Transactions on Energy Conversion, vol. 23, pp. 997–1004, Dec. 2008.

[10] "IEEE Standard Test Procedure for Polyphase Induction Motors and Generators," IEEE Std 112-2017 (Revision of IEEE Std 112-2004), pp. 1–115, Feb. 2018

[11] S A. Odhano, *et al.*, "Parameter Identification and Self-Commissioning in AC Motor Drives: A Technology Status Review", IEEE Transactions on Power Electronics, vol. 34, pp. 3603–3614, April 2019.

[12] H.A. Toliyat, E. Levi, and M. Raina, "A review of RFO induction motor parameter estimation techniques", IEEE Transactions on Energy Conversion, vol. 18, pp. 271–283, June 2003.

[13] D.M. Reed, H.F. Hofmann, and J. Sun, "Offline Identification of Induction Machine Parameters With Core Loss Estimation Using the Stator Current Locus", IEEE Transactions on Energy Conversion, vol. 31, pp. 1549–1558, Dec. 2016.

[14] M. Richter, B. Brendle, M. Stiegeler, M. Mendes, and H. Kabza, "Flux maps for an efficiency-optimal operation of asynchronous machines in hybrid electric vehicles", IEEE Vehicle Power and Propulsion Conference, pp. 1–6, Sept. 2011.

[15] W. Leonhard, "Control of Electrical Drives", Springer Science & Business Media, Aug. 2001.

[16] I. R. Bojoi, E. Armando, G. Pellegrino and S. G. Rosu, "Self-commissioning of inverter nonlinear effects in AC drives," 2012 IEEE International Energy Conference and Exhibition (ENERGYCON), 2012, pp. 213–218.

[17] G. Pellegrino, R. Bojoi and P. Guglielmi, "Unified Direct-Flux Vector Control for AC motor drives," 2010 IEEE Energy Conversion Congress and Exposition, 2010, pp. 1150–1157.